ADVANCED MATERIALS INTERFACES
Open Access
www.advmatinterfaces.de

Deactivation of Partially (dis)Charged LNMO in Contact with Water by Electrochemical Protonation of $Li_{(1-x)}Ni_{0.5}Mn_{1.5}O_4$

Andrea I. Pitillas, Louis L. De Taeye, and Philippe M. Vereecken**

The development of water-based composite cathode slurries for Li-ion batteries is hindered by adverse interactions between the battery active material and water. Insights into interactions between H_2O and $LiNi_{0.5}Mn_{1.5}O_4$ (LNMO) are studied using a thin-film model system. The reactivity of this active material with H_2O is evaluated at different lithiation states, showing that protonation of the active material in aqueous environments is electrochemically driven, rather than a chemical Li^+/H^+ ion exchange reaction. The electrochemically driven mechanism describing the protonation of LNMO is only present when the material is in its partially delithiated form. These findings suggest it is possible to cast this material from an aqueous precursor when lithiated, as long as there are no traces of it when the electrochemical delithiation (cell charging) is carried out.

1. Introduction

$LiNi_{0.5}Mn_{1.5}O_4$ (LNMO) is a next generation cathode material with a competitive energy density and ability to deliver high power density due to its high working potential (≈4.7V vs Li^+/Li) and fast lithium ion conduction.[1] LNMO has better thermal stability[2] than the high Ni variants of $LiNi_xMn_yCo_zO_2$ (NMC) and is safer due to the absence of oxygen release at high potentials.[3,4] Further, LNMO has a lower cost[2,5,6] as it does not contain cobalt and has a lower Ni content than the most energy dense NMC materials. Some technical shortcomings still prevent commercial deployment of the material. A first barrier that persists for spinel cathode materials such as $LiMn_2O_4$ (LMO) or LNMO is its severe capacity fading linked to transition metal dissolution (TMD).[7] Second, the material operates at a high working potential leading to electrochemical breakdown of all commonly used electrolyte solutions at these elevated potentials (>4.5V vs Li^+/Li) linked to oxidation of both the salt and solvent.[8] The two degradation mechanisms are intricately linked to one another, as TMD is accelerated by the presence of protons,[9,10] which can form as a by-product of (electro)chemical decomposition of the electrolyte solution.[11]

Aside from reactions with the electrolyte during cell operation, the material can interact with solvents during slurry casting. In particular, for aqueous processing, there is a risk of side-reactions between the water-based slurry and the battery active material. The focal point of this article is the interaction between water and LNMO. Cathode active material are generally (electro)chemically unstable in contact with aqueous solutions. This has been attributed to both redox processes (such as disproportionation of LMO) and/or cation exchange processes (Li^+/H^+ ion exchange reaction).[12] The latter has been studied extensively for $LiNi_xMn_yCo_zO_2$. In NMC, the ion exchange process is linked to either a chemical and/or an electrochemically driven process during which Li^+ is extracted from the cathode material with coinciding H^+ insertion.[13] It is worthwhile to assess the existing hypotheses for ion exchange in NMC, before evaluating the same in LNMO.

Starting with the chemical process: this process is mainly observed in high pH (alkaline) solutions. Here, OH^- can strongly absorb onto the surface of materials such as NCA and NMC.[14] The hydroxyl group coordinates strongly with Li^+ or the transition metal, leading to concomitant protonation of the active material and LiOH formation on the active material surface. Overall, the redox state of the transition metals is never altered in this process. The LiOH formed on the surface can subsequently react with CO_2 to form Li_2CO_3:

$$Li^+ + H_2O \rightarrow H^+ + LiOH \quad (1a)$$

$$LiOH + CO_2 \rightarrow LiHCO_3 \quad (1b)$$

$$LiOH + LiHCO_3 \rightarrow H_2O + Li_2CO_3 \quad (1c)$$

Through these reactions, the process can continue until the surface is passivated by the stable Li_2CO_3 film.

The second mechanism for ion exchange is an *electro*chemical process. Herein, the cathode active material is delithiated with

A. I. Pitillas, L. L. De Taeye, P. M. Vereecken
IMEC
Kapeldreef 75, Leuven 3001, Belgium
E-mail: louis.detaeye@imec.be; philippe.vereecken@imec.be
A. I. Pitillas, P. M. Vereecken
KU Leuven Centre for Membrane Separations, Adsorption Catalysis, and Spectroscopy for Sustainable Solutions
Celestijnenlaan 200F - box 2454, Leuven 3001, Belgium
The ORCID identification number(s) for the author(s) of this article can be found under https://doi.org/10.1002/admi.202400003

DOI: 10.1002/admi.202400003

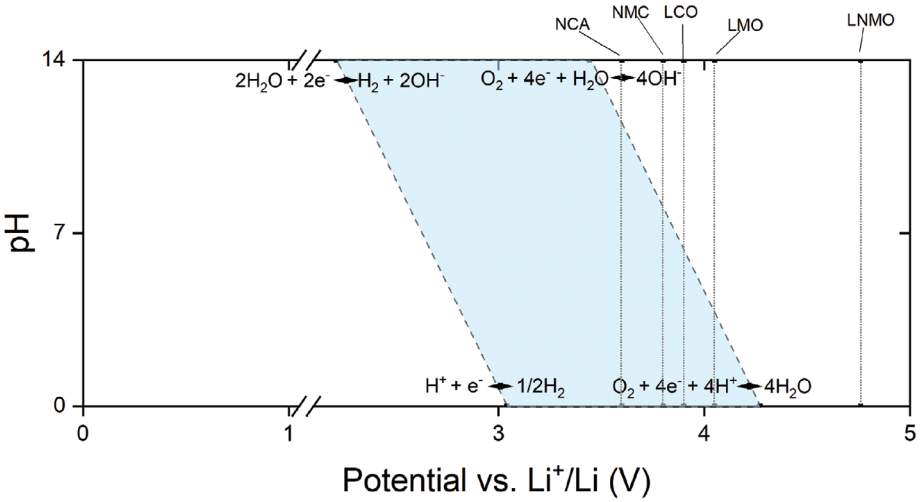

Figure 1. Graphical summarizes the formal potentials a selection of commonly used cathodes:[16] NCA (3.6 V), NMC (3.8), LCO (3.9 V), LMO (4 V), and LNMO (4.7 V), and the electrochemical stability window of water at pH between 0 (3.04–4.27 V vs Li^+/Li) and 14 (2.21–3.44 V vs Li^+/Li), indicated by the blue box.

coinciding oxidation of the transition metal. According to literature, water/proton reduction is the reductive counterpart of the redox reaction.[14,15] However, careful evaluation of the position of the electrochemical equilibrium potentials associated with water reduction and commonly used cathode active materials (as shown in **Figure 1**), shows that this is unlikely. Nonetheless, an inverse relationship between a material's redox potential and stability in ambient atmosphere exists.[14,15] A more likely reduction process would be oxygen reduction, as the equilibrium potential of this reaction is positioned more closely to the insertion potentials of NMC or NCA. For LNMO, these same (chemical and electrochemical) processes have been hypothesized.[17] In their work, a shift in the pH is observed as LNMO is submerged in an aqueous solution. This was associated to both manganese dissolution and lithium-proton exchange. However, the composition of LNMO was not analyzed after long-term storage in this solution, and the delithiation is only inferred based on the pH change.

In this article, LNMO thin-films are used as a test platform. This system has only a single active material/electrolyte interface and contains no passive components, such as carbon additives or binders, greatly simplifying interpretation of the results. The interaction between water and LNMO and its impact on the electrochemical performance of LNMO is evaluated at two different lithiation states. Using a thin-film further enables techniques capable of measuring the Li^+ and H^+ concentration in the active material such as ERD. The comparative analysis shows that the interactions with water strongly depend on the lithiation state of the material, indicating the mechanism is *electrochemically* driven. Based on the observed phenomena, a mechanistic description of the interaction is postulated.

2. Experimental Section

2.1. Sputter Deposition and Annealing Conditions

The LNMO thin films were deposited by RF-sputtering using a 3'' target from Neyco (LNMO, purity 99.9%). The depositions were done at 55 W under Ar flow at 3 mTorr for 2h in a Kurt J. Lesker Company sputter tool connected to a glovebox. LNMO thin-films were deposited on a 10 nm Pt/oxidized-10 nm Ti/100 nm SiO_2/Si) substrate. This substrate was prepared using a commercial 100 nm thermal SiO_2 coated wafer from Si-Mat as a substrate. A 10 nm Ti layer was deposited by evaporation using an Alcatel tool, followed by annealing at 800°C in O_2 for 20 min to oxidize it using an Annealsys oven As-One. A 10 nm Pt film was evaporated on top of the oxidized titanium thin-film using a PLS-A evaporation tool. The deposited LNMO thin films were annealed under ambient atmosphere at 700 °C for 1 h with a 5 °C min^{-1} ramping rate in a Nabertherm oven. After the annealing process, the sample was cooled down at a controlled rate of 4°C min^{-1}.

2.2. LNMO Thin-Film Material Characterization

Structural characterization was done using a Philips Panalytical X' Pert XRD system equipped with a Cu Kα X-ray source (λ = 1.5406 Å) and a linear X-ray detector. The cation ordering was studied by Raman spectroscopy using a Horiba Jobin-Yvon HR800 with a laser of 532 nm and using a 25%ND filter and that had a grating of 1800 grooves/mm. The recorded spectrum was measured with double exposure (2 × 25s) with a spike filter to eliminate the cosmic peaks. The film composition was determined by Time of Flight - Energy Elastic Recoil Detection and Analysis (TOF-E ERDA) using a 6SDH tandem accelerator with a maximum terminal voltage of 2.0 MV from National Electrostatics Corporation (NEC), Middleton (WI), U.S.A.[18,19] The measurements were carried out using an iodine ($^{127}I^{7+}$) impinging beam accelerated to 13.636 MeV to improve mass resolution and separate Ni and Mn in the measured spectra. SEM pictures were obtained with a FEI Verios at a current of 0.1 nA and voltage of 5 kV. Particle-induced X-ray emission (PIXE) was used in order to more accurately determine the Mn/Ni ratio present in the samples. PIXE measurements were recorded using $^1H^+$ (2.3 MeV),

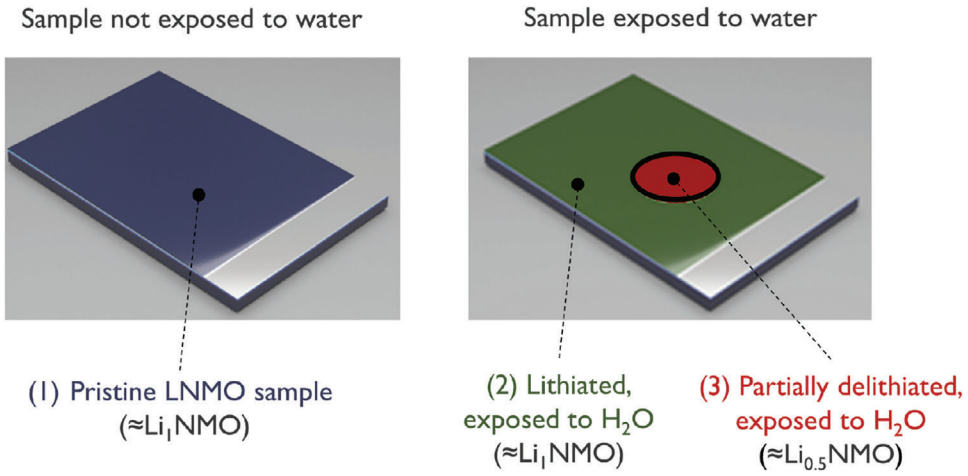

Figure 2. Different LNMO samples prepared to study the replacement of Li^+ by H^+ in LNMO when this is in contact with water. Drawing depicting the different samples prepared, colors given to the samples for identification, 1) pristine (lithiated) LNMO thin-film, 2) a pristine (lithiated), exposed to H_2O thin-film, and 3) a delithiated LNMO, exposed to H_2O.

with a sample normal, using a 30 mm^2 detector of ultra-low energy with a energy resolution of nominal 160 eV.The K emission lies were used for the Mn and Ni, while the L emission lines were used for Pt.

2.3. Electrochemical Characterization

The electrochemical characterization was done in a glovebox under an argon atmosphere (O_2 and H_2O ⩽ 1ppm) using a 3-electrode Teflon cell clamped on the cathode thin film using an O-ring with an inner area (equal to the area of LNMO to the electrolyte) of 0.63 cm^2 as shown depicted in schematically in Figure S1a (Supporting Information). Two lithium metal strips were used as counter and reference electrodes, while the $LiNi_{0.5}Mn_{1.5}O_4$ thin-film was set as the working electrode. All electrochemical experiments were performed using an in-house electrolyte. The electrolyte was a 1M $LiClO_4$ (battery grade, dry, with a purity of 99.99% from Sigma–Aldrich) in propylene carbonate (PC) (anhydrous from 99.7% from Sigma–Aldrich).

2.4. LNMO Delithiation Pretreatment Conditions

For some of the experiments, an electrochemical (de)lithiation pretreatment was carried out. The pretreatment consisted of one constant-current charge–discharge cycle (≈ 1 C = 5 μA cm^{-2}) to check the performance of the cathodes, followed by a constant current charge at the same current, up to a potential 4.8V versus Li^+/Li. This conditions corresponds to complete delithiation. However, in these thin-films, any degradation caused by the electrolyte will lead to self-discharge (i.e. lithiation of LNMO). After delithiation, the sample was immediately rinsed in PC to minimize self-discharge by the electrolyte. However, some partial lithiation remains inevitable. Therefore, the LNMO is described as partially delithiated. After rinsing, the sample was loaded into a Buchi oven inside a glovebox and dried under vacuum at 80°C overnight to remove any solvent traces. The cleaned sample was subsequently exposed to H_2O. Exposure to water was done outside of the glovebox. The sample was dipped in water for 1 min and dried at 100 °C in vacuum to get rid of any remaining water traces. The time in which the samples were kept outside the glovebox was minimized, and the samples were immediately placed back in the glovebox after the exposure and drying steps. For these samples, the two different areas studied are indicated schematically as the delithiated and pristine areas (see **Figure 2** below - Note that the color change between the different lithiation states and upon water exposure is not as clear as depicted in the schematic representation, this is just added for clarity).

3. Results and Discussion

3.1. Thin-Film Deposition and Characterization

LNMO thin films were fabricated using RF-sputtering. The as-deposited films were thermally annealed to form the desired spinel phase of LNMO. **Figure 3** summarizes the results of structural analysis by means of X-ray diffraction (XRD), Raman spectroscopy and SEM of LNMO deposited on a 10 nmPt/10 nm-oxidized Ti/100 nm SiO_2/Si. XRD confirmed the crystalline structure associated with the cubic spinel phase (Figure 3a). The cubic spinel phase exhibits two types of cation ordering, ordered LNMO (P_{4332}) and disordered LNMO (Fd-3m), which are hard to distinguish from diffraction patterns obtained using XRD. Raman spectroscopy was used to determine the cation ordering of the LNMO thin films. After annealing, the characteristic peaks of disordered LNMO (Fd-3m) around 164, 397, 496, 597, and 637 cm^{-1} (Figure 3b) were observed, which are in good agreement with the reported values in literature. The SEM images of (Figure 3c) shows a ≈70 nm thin film with a continuous and closed polycrystalline morphology.

The chemical composition of the LNMO thin films was determined using two complementary analysis techniques. Time of Flight - Energy Elastic Recoil Detection and Analysis (ToF-E ERDA) and Particle-Induced X-ray Emission (PIXE) were used to determine the Li, Ni, Mn, and O atomic fractions. The Ni

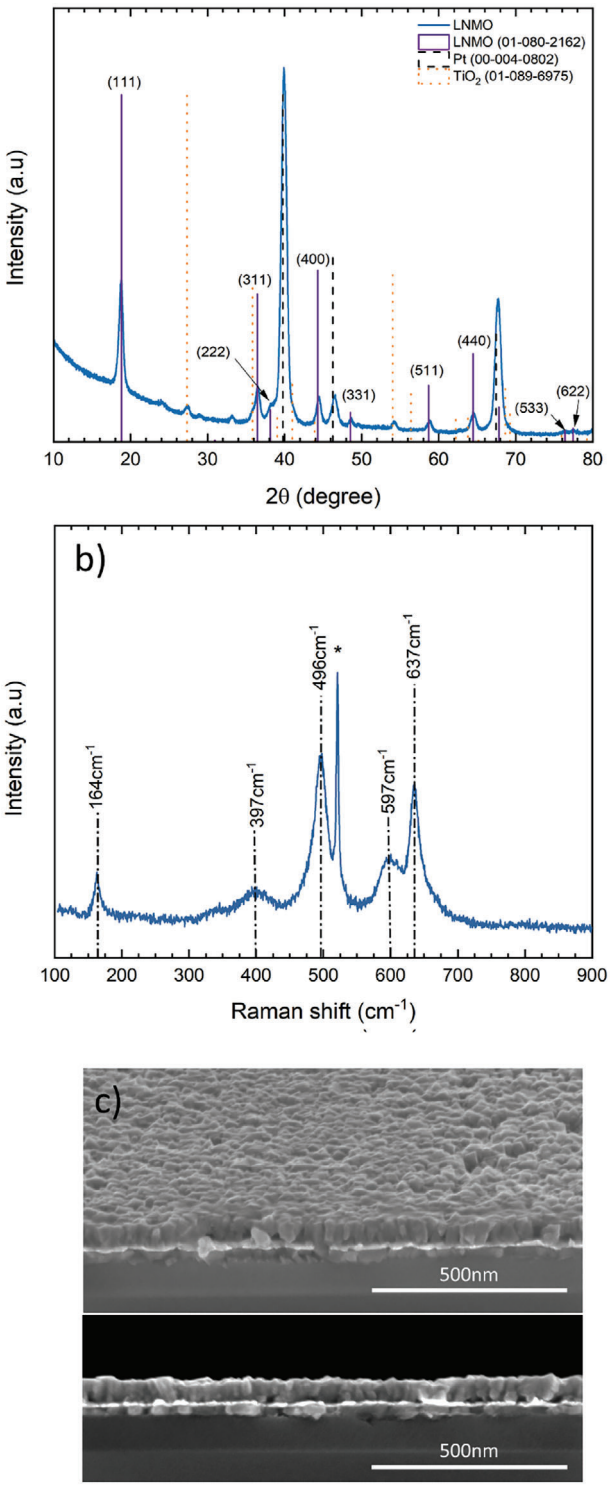

Figure 3. Structural analysis of the LNMO thin films prepared by RF-sputtering on 10 nmPt/30 nmTiO_2/100 nmSiO_2/Si substrates prepared after annealing in air at 700 °C. a)LNMO thin film XRD pattern with the peaks assigned to the LNMO Miller indices, according to the reference file 80-2162 and reference patterns for the substrate Pt (00-004-0802) and TiO_2 (01-089-6975).b)Raman spectra of a pristine sample showing a $Fd\bar{3}m$ cation ordering, where * corresponds to the Si peak from the substrate. c)SEM Cross-section of a ≈ 70nm LNMO thin film showing continuous film with columnar grain morphology.

content cannot be quantified accurately by ToF-E ERDA alone, due to the low detection efficiency of recoiled nickel events under the experimental conditions used. Consequently, PIXE was used to determine the atomic Mn to Ni ratio more accurately. This ratio was then used to correct the underestimated Ni content from TOF-E ERDA. The Mn/Ni ratio was found to be 2.7 (see **Table 1**), close to the expected ratio (Mn/Ni = 3) and in accordance with the previously reported ratio of 2.7 for sputtered LNMO thin-films.[20]

3.2. Electrochemical Characterization of LNMO After Water Exposure at Different Lithiation States

The mechanism behind replacement of Li^+ by H^+ was evaluated on lithiated (x = 1) and partially delithiated (× ~0.5) $Li_xNi_{0.5}Mn_{1.5}O_4$ thin films. These samples were exposed to water and compared to a pristine sample (i.e., as-deposited LNMO with x = 1, which was not exposed to water) in terms of electrochemical performance and composition. The samples are schematically represented in Figure 3. The partially delithiated area is confined to the surface inside the O-ring. For more details on the measurement set-up see Figure S1 (Supporting Information). For ease of reading, the following labels will be used throughout the text: pLNMO (blue area, as-deposited), eL1NMO (green area, as-deposited, exposed to water), and eL0.5NMO (red area, delithiated to x = 0.5, exposed to water). The electrochemical measurements on the three types of samples comprised cyclic voltammetry, followed by galvanostatic charge–discharge to evaluate how water exposure altered the electrochemical performance.

The resulting CV curves are shown in **Figure 4**. The pristine reference sample (pLNMO) shows the characteristic double peak for LNMO at 4.7 and 4.78 V versus Li+/Li corresponding to oxidation of Ni^{+II} to Ni^{+III}, and Ni^{+III} to Ni^{+IV}, respectively. The inset highlights a small current signal in the 4 V region. This is indicative of some redox activity associated with Mn, which can oxidize from Mn^{+III} to Mn^{+IV} in disordered LMO. A comparison of the pLNMO sample and the lithiated sample exposed to H_2O (eL1NMO) is shown in Figure 4a. Only minor changes can be observed in the cyclic voltammogram, such as a slight shift of the main peaks in the 4.75 V region toward higher potentials and a slight decrease of the anodic peak currents for the water treated sample. The small anodic peak observed in the 4 V-region is observed to shift to lower potentials and a small cathodic peak becomes more distinguishable. The sample that was delithiated prior to exposure to H_2O (eL0.5NMO) is affected more severely by this exposure. Here, LNMO is nearly completely electrochemically inactive, with no discernible anodic or cathodic peaks in the CV.

Following the cyclic voltammetry, galvanostatic charge–discharge cycling was performed (see Figure 4b,c). Overall,

Table 1. Composition based only on ERD and composition based on corrected ERD by PIXE for nickel content correction.

		Li	O	Mn	Ni
ERD	Dis.	0.127 ±0.007	0.601± 0.020	0.209 ± 0.011	0.063[a)]
ERD+PIXE	Dis.	0.125±0.007	0.592±0.021	0.206 ±0.011	0.078[a)]

[a)] Error could not be estimated for Ni.

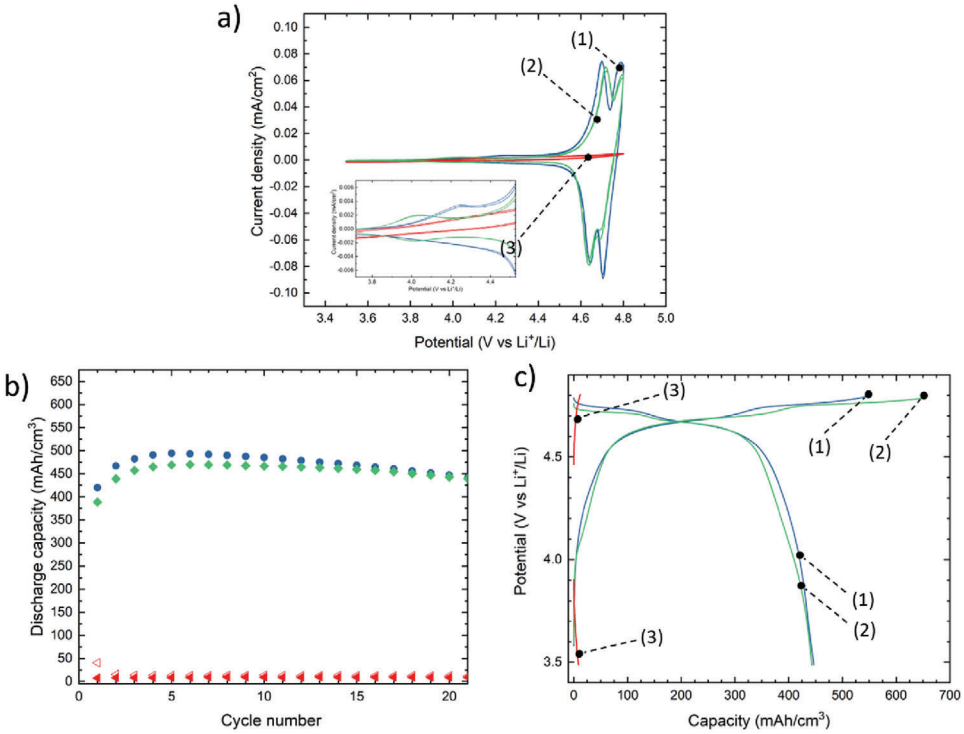

Figure 4. Lithiation and delithiation behavior in 1M $LiClO_4$ in PC. a) Cyclic voltammograms at 1mV s^{-1} (2nd and 3rd cycles). b) Discharge (filled symbols) capacity of the pristine sample (○), lithiated, exposed to H_2O (◇) and delithiated, exposed to H_20 (◁) cycled at 1 C. c) Charge and discharge potential-capacity curves for cycle 20 at ≈ 1 C (≈5 μA cm^{-2}).

from the discharge capacities as a function of the cycle number, the pLNMO and eL1NMO behave similarly. In the charge–discharge curves presented in Figure 4c, two plateaus are observed at 4.7 and 4.78V versus Li^+/Li, which correspond to the twin peaks observed in the cyclic voltammogram. A disparity is observed between the charge and discharge capacities (see Figure 4c; Figure S4, Supporting Information) between the two samples. For the pLNMO sample, charge and discharge capacities of 560 and 440 mAh cm^{-3} were measured, respectively. The same discharge capacity is measured after water exposure, but a higher charge capacity of 640 mAh cm^{-3}, is observed. The significant difference between charge and discharge capacity is the consequence of oxidation of the organic electrolyte at these high potentials. In contrast, no (de)lithiation plateaus are observed in the eL0.5NMO, showing that the water exposure results in an electrochemically inactive film.

3.3. Physico-Chemical Analysis of Water Exposed LNMO Thin-Films

The presence of either H^+ or Li^+ within the different LNMO thin films was studied by Time-of-Flight-Energy Elastic Recoil Detection Analysis (ToF-E ERDA). **Figure 5a–c** shows the ToF-E ERDA depth profiles for the pLNMO, eL1NMO, and eL0.5NMO. Hydrogen is detected at the surface regardless of the lithiation state of the sample and whether or not the samples were exposed to water. This is linked either to hydrocarbon contamination at the sample surface[20] or/and to protonation of the dangling bonds at the surface, that is, hydroxyl surface groups.[21]

Notably, the hydrogen concentration significantly differs in the bulk of the thin films for the three samples. The pLNMO sample showed a negligible proton count in the bulk of the thin film, as observed from Figure 5a and **Table 2** with an average H/O ratio of 0.013, which can be considered a baseline value for background contamination. For the eL1NMO (see Figure 5b and Table 2), the hydrogen content increased slightly while the lithium content decreased accordingly, suggesting minor Li^+ to H^+ exchange might have taken place. However, given that the Li/O ratio decreased only by ≈ 0.01, while the H/O increased by ≈ 0.01, this indicates that this effect is negligible. This is in good agreement with

Table 2. Theoretical ratio expected assuming a stoichiometric LNMO (i.e., $LiNi_{0.5}Mn_{1.5}O_4$) versus experimental ratios of the different areas pristine, lithiated, exposed to H_2O and delithiated, exposed to H_2O. The ratios were calculated by dividing the fractions obtain for each of the elements within the bulk ($180{\cdot}10^{15}$ to $410{\cdot}10^{15}$ at cm^{-2}) of the layer. The lithium content in the table has been corrected taking into consideration the abundance of ^6Li.

Ratios	Theoretical	Pristine	Lithiated, exposed to H_2O	Delithiated, exposed to H_2O
H/O	0.00	0.013 ± 0.002	0.021 ± 0.002	0.107 ± 0.011
Li/O	0.25	0.249 ± 0.009	0.237 ± 0.009	0.107 ± 0.004

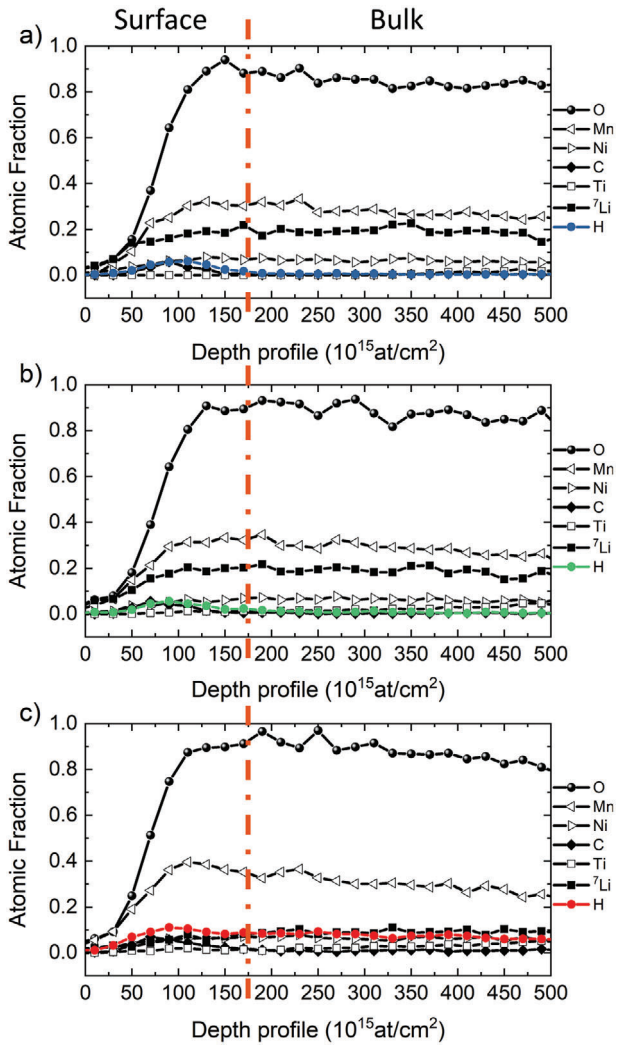

Figure 5. TOF-E ERDA depth profile of LNMO: a) Pristine: As sputtered after annealing. b) After annealing, exposed to H_2O. c) After annealing, electrochemically delithiated and exposed to H_2O. Note, the lithium content represented in this graphs is only ^{7}Li.

previously reported theoretical predictions that the Li^+/H^+ exchange reaction is only slightly favorable ($\Delta G° = -0.2$ eV) for spinel materials, as has been reported for $LiMn_2O_4$ (LMO).[22]

Interestingly, the eL0.5NMO sample exposed to water (see Figure 5c) shows a large bulk proton concentration throughout the film, suggesting H^+ insertion into the partially delithiated $Li_xH_yNi_{0.5}Mn_{1.5}O_4$ film takes place. The Li/O ratio of 0.107 corresponds to a Li-ion state-of-charge x = 0.43, meaning that the sample was not fully delithiated, as expected, due to severe electrolyte decomposition during and after the galvanic step at 1 C. The H/O ratio was also 0.107, corresponding similarly to a protonation state-of-charge of y = 0.43 (see Figure 5 and Table 2). The total state-of-charge of the samples is 0.86, close to 1, indicating an almost fully half lithiated, half protonated thin film ($Li_{0.43}H_{0.43}$NMO).

As the lithiated sample exposed to water did not show a significant hydrogen concentration in-depth, the degradation mechanism of LNMO by a Li^+/H^+ ion exchange reaction can be excluded. This is contrary to what happens to other cathode materials such as for example NMC. However, the electrochemically delithiated sample, exposed to water, showed a significant concentration of hydrogen in the whole depth of the thin film, indicating an alternative mechanism is causing protonation.

Raman spectroscopy was performed on the same set of samples as ERD to detect traces of other compounds being formed on the electrode surface (e.g., carbonate and hydroxide compounds)[23] after exposure of two of the samples to water, as well as to observe any changes in the LNMO structure itself after water exposure. The comparison of the Raman spectra for the pristine sample and the eL1NMO (see **Figure** 6a) shows no significant differences between the two spectra, nor the presence of additional bands corresponding to carbonates or hydroxides after water exposure. Hence, this suggests that the slight electrochemical differences for the eL1NMO might stem from small surface reconstruction. The Raman spectrum agrees with the ERD results, showing Li^+/H^+ exchange is negligible in LNMO when the material is fully lithiated. The results of ERD and Raman suggest that fully lithiated LNMO can be processed in aqueous or atmospheric conditions without being detrimental effects to the electrochemical performance or composition of the material.

More pronounced differences can be observed between the eL0.5NMO and the pristine samples (see Figure 6b). While no carbonate and hydroxide compounds were detected for the exposed sample, the crystalline structure of the LNMO was to

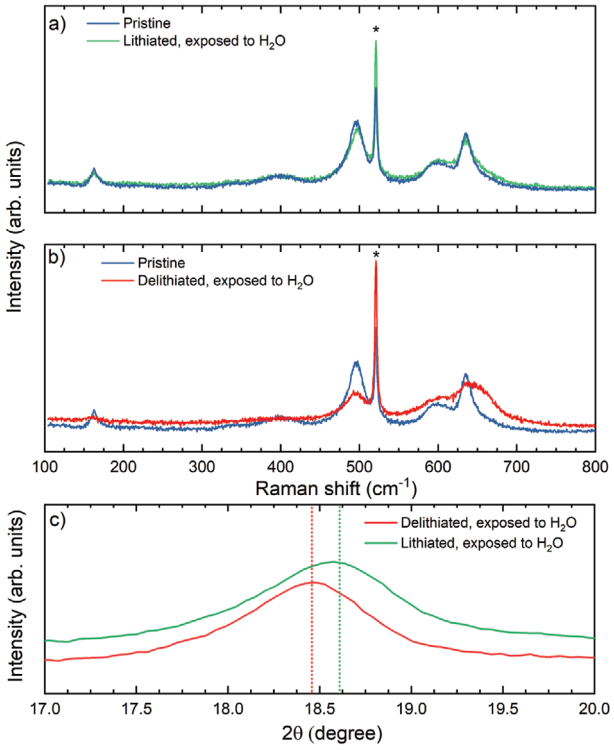

Figure 6. Raman spectras a) Pristine versus lithiated, exposed to H_2O. b) Pristine versus delithiated, exposed to H_2O, and c) a comparison of the (111) X-ray diffraction peak of LNMO after water exposure at different lithiation states.

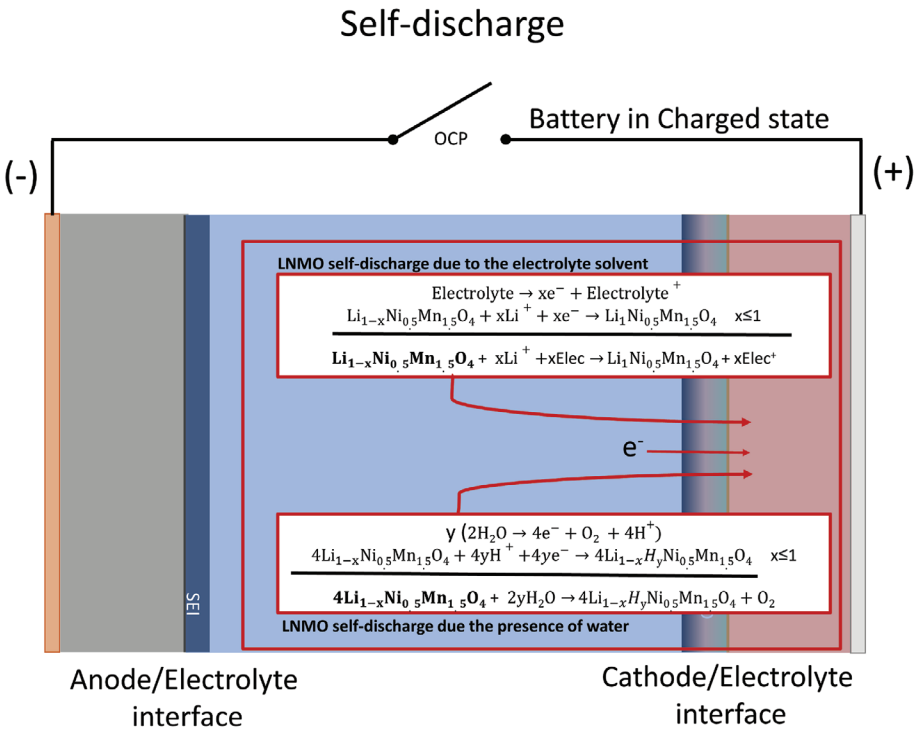

Figure 7. Figure depicting the commonly postulated self-discharge of high-voltage cathodes in the presence of an electrolyte versus the self-discharge mechanism in water.

be significantly affected. In this case, a clear broadening of the bands can be observed. This can be linked either to proton insertion which introduces atomic disorder and thus band broadening, together with shifts in peak positions.[24] The bands in between 570 and 650 are related to the Mn-O modes in the MnO_6 octahedron.[25] The presence of broad bands suggests induced structural changes. For instance, this can be linked to the appearance of a spinel phase of lower symmetry[25] (e.g., λ-MnO_2).[26]

Finally, Figure 6c shows a comparison of the (111) peak of LNMO measured by XRD after water exposure at different lithiation states. Proton insertion can impact the lattice parameter of transition metal oxide active materials. This is well documented for layered structures.[27] The impact of the protonation on the lattice constant will be extracted from this (111) peak. A peak shift of 0.09° from 18.57° for the eL1NMO to 18.48° for the eL0.5NMO was observed between the two samples. Partially protonated $Li_{0.43}H_{0.43}$NMO has a lattice constant of 8.31 Å, slightly larger than the lithiated counterpart with a lattice constant of 8.27 Å.

3.4. Mechanistic Description of Electrochemical Protonation

The protonation of LNMO is not driven by an ion-exchange reaction. Based on the observations, we postulate an electrochemical mechanism driving protonation, as described in Equation (2).

$$4Li_{1-x}Mn_{1.5}Ni_{0.5}O_4 + 4yH^+ + 4ye^- \leftrightarrow 4Li_{1-x}H_yMn_{1.5}Ni_{0.5}O_4 \quad (2)$$

Both proton and electrons are released upon breakdown of water as:

$$y(2H_2O - 4e^- \leftrightarrow O_2 + 4H^+) \quad (3)$$

The anodic breakdown voltage of water w.r.t. Li^+/Li depends on the pH and reaches a maximum value of approximately 4.28V versus Li^+/Li (equivalent to 1.23V vs SHE) for pH = 0. Consequently, LNMO will spontaneously decompose water upon delithiation, as the potential exceeds 4.75V versus Li^+/Li. Combining both reactions leads to the overall electrochemically driven protonation reaction:

$$4Li_{1-x}Mn_{1.5}Ni_{0.5}O_4 + 2yH_2O \leftrightarrow 4Li_{1-x}H_yMn_{1.5}Ni_{0.5}O_4 + yO_2 \quad (4)$$

The mechanism is also schematically depicted in **Figure 7**.

An alternative source of electrons at the LNMO surface is the oxidative breakdown of the electrolyte itself. On the one hand, this can lead to spontaneous lithiation of the LNMO (i.e., self-discharge), on the other hand, it could lead to protonation of the solution by forming the free H^+. Conseqeuntly, electrolyte breakdown at high voltage cathodes (once delithiated) has a second order effect. Both protons are generated and the electrolyte is reduced during electrolyte oxidation. The electrogenerated protons are inserted into the active material and render the material inert.

4. Conclusion

Protonation of LNMO, a high energy-density cathode material, upon exposure to water was studied in this work. It is generally

recognized that water exposure has a detrimental effect on cell performance and is a serious issue for Li-ion battery cell manufacturing using aqueous processes. This is generally ascribed to an ion exchange process in which Li^+-ion are exchanged for H^+. To study whether these protonation/replacement reactions occur in LNMO, we have developed a new approach using a thin-film model system. A planar LNMO thin-film at two different states of charge was brought in contact with H_2O. By combining XRD, ERD, Raman, and electrochemical characterization, we showed that the Li^+/H^+ does not affect LNMO when this material is fully lithiated. However, proton insertion and the coinciding reduction of Ni are clearly observed in delithiated LNMO upon water exposure. The protonation is electrochemically driven, and only happens at for charged (delithiated state). This is in contrast to the (partially) chemical nature of the H^+/Li^+ exchange reactions in for example, NMC. Protonation of the L_xNMO into H_yLi_xNMO makes it electrochemically inactive as the protons are much more strongly bonded to the oxygen in the spinel lattice. The fundamental mechanisms prescribing decomposition of LNMO upon exposure to water were unravelled. The core finding shows that protonation of LNMO does not happen spontaneously when lithiated LNMO is exposed to water. This finding suggests that if LNMO is processed from an aqueous solution, there will be no (electro)chemical degradation of the material linked to the interaction with water itself. However, trace amounts of water in the electrode can still de-activate the LNMO through protonation. Consequently, the electrode slurry drying process remains a critical step in the manufacturing. Electrolyte additives or artificial interface coatings are an interesting route to create a more stable cathode-electrolyte interface (CEI), which suppresses side reactions on the electrode surface. However, many of the protective coatings developed are based either on deposition processes using aqueous solutions,[28,29] or water vapor as a co-reactant, as in atomic layer deposition.[30] This work shows that these methods can only be applied to fully lithiated LNMO. A thin-film model system is an excellent tool to study these modification to the active material surface as well.

Supporting Information

Supporting Information is available from the Wiley Online Library or from the author.

Acknowledgements

This project has received funding from the European Union's Horizon 2020 research and innovation program under the Marie Skłodowska-Curie grant agreement No. 765378. Kurt J. Lesker Company is acknowledge for collaboration on the Mini SPECTROS and Nano 36 glovebox cluster sputtering tool. The authors thanks Praveen Dara for the TOF-E ERDA measurement and Stefanie Sergeant for the Raman measurement and Cole Smith for the XRD measurment.

Conflict of Interest

The authors declare no conflict of interest.

Data Availability Statement

The data that support the findings of this study are available from the corresponding author upon reasonable request.

Keywords

cathode, Li-ion, LNMO, proton exchange, water

Received: January 10, 2024
Revised: March 14, 2024
Published online: April 18, 2024

[1] J. L. Allen, B. A. Crear, R. Choudhury, M. J. Wang, D. T. Tran, L. Ma, P. M. Piccoli, J. Sakamoto, J. Wolfenstine, *Molecules* **2021**, *26*, 9.
[2] W. Li, Y. G. Cho, W. Yao, Y. Li, A. Cronk, R. Shimizu, M. A. Schroeder, Y. Fu, F. Zou, V. Battaglia, A. Manthiram, M. Zhang, Y. S. Meng, *J. Power Sources* **2020**, *473*, 228579.
[3] R. Jung, M. Metzger, F. Maglia, C. Stinner, H. A. Gasteiger, *J. Electrochem. Soc.* **2017**, *164*, A1361.
[4] J. Chen, Y. Yang, Y. Tang, Y. Wang, H. Li, X. Xiao, S. Wang, M. S. D. Darma, M. Etter, A. Missyul, A. Tayal, M. Knapp, H. Ehrenberg, S. Indris, W. Hua, *Adv. Funct. Mater.* **2023**, *33*, 2211515.
[5] M. Wentker, M. Greenwood, J. Leker, *Energies* **2019**, *12*, 1.
[6] N. Muralidharan, E. C. Self, M. Dixit, Z. Du, R. Essehli, R. Amin, J. Nanda, I. Belharouak, *Adv. Energy Mater.* **2022**, *12*, 1.
[7] C. Zhan, T. Wu, J. Lu, K. Amine, *Energy Environ. Sci.* **2018**, *11*, 243.
[8] W.-h. Hou, Y. Lu, Y. Ou, P. Zhou, S. Yan, X. He, X. Geng, K. Liu, *Trans. Tianjin Univ.* **2023**, *29*, 120.
[9] R. Sahore, D. C. O'Hanlon, A. Tornheim, C.-W. Lee, J. C. Garcia, H. Iddir, M. Balasubramanian, I. Bloom, *J. Electrochem. Soc.* **2020**, *167*, 020513.
[10] A. Bhandari, J. Bhattacharya, *J. Electrochem. Soc.* **2017**, *164*, A106.
[11] C. G. Barlowz, *Electrochem. Solid-State Lett.* **1999**, *2*, 362.
[12] I. A. Shkrob, J. A. Gilbert, P. J. Phillips, R. Klie, R. T. Haasch, J. Bareño, D. P. Abraham, *J. Electrochem. Soc.* **2017**, *164*, A1489.
[13] I. Hamam, N. Zhang, A. Liu, M. B. Johnson, J. R. Dahn, *J. Electrochem. Soc.* **2020**, *167*, 130521.
[14] N. V. Faenza, L. Bruce, Z. W. Lebens-Higgins, I. Plitz, N. Pereira, L. F. J. Piper, G. G. Amatucci, *J. Electrochem. Soc.* **2017**, *164*, A3727.
[15] W. Li, W. R. McKinnon, J. R. Dahn, *J. Electrochem. Soc.* **1994**, *141*, 2310.
[16] F. Wu, J. Maier, Y. Yu, *Chem. Soc. Rev.* **2020**, *49*, 1569.
[17] I. Dienwiebel, M. Diehl, B. Heidrich, X. Yang, M. Winter, M. Börner, *Adv. Energy Sustainabil. Res.* **2021**, *2*, 2100075.
[18] J. Meersschaut, W. Vandervorst, *Nucl. Instrum. Methods Phys. Res., Sect. B* **2017**, *406*, 25.
[19] J. Meersschaut, G. Laricchiuta, T. Sajavaara, W. Vandervorst, *Nucl. Instrum. Methods Phys. Res., Sect. B* **2016**, *371*, 153.
[20] L. Baggetto, R. R. Unocic, N. J. Dudney, G. M. Veith, *J. Power Sources* **2012**, *211*, 108.
[21] N. N. Intan, K. Klyukin, V. Alexandrov, *J. Electrochem. Soc.* **2018**, *165*, 1099.
[22] R. Benedek, M. M. Thackeray, A. Van De Walle, *Chem. Mater.* **2008**, *20*, 5485.
[23] R. Jung, R. Morasch, P. Karayaylali, K. Phillips, F. Maglia, C. Stinner, Y. Shao-Horn, H. A. Gasteiger, *J. Electrochem. Soc.* **2018**, *165*, A132.
[24] J. D. Pasteris, O. Beyssac, *Elements* **2020**, *16*, 87.
[25] K. Saravanan, A. Jarry, R. Kostecki, G. Chen, *Sci. Rep.* **2015**, *5*, 1.
[26] Y. Talyosef, B. Markovsky, G. Salitra, D. Aurbach, H.-J. Kim, S. Choi, *J. Power Sources* **2005**, *146*, 664.

[27] W. Hua, X. Yang, N. P. Casati, L. Liu, S. Wang, V. Baran, M. Knapp, H. Ehrenberg, S. Indris, *eScience* **2022**, *2*, 183.
[28] B. Huang, X. Li, Z. Wang, H. Guo, X. Xiong, J. Wang, *J. Alloys Compd.* **2014**, *583*, 313.
[29] L. Li, Z. Chen, Q. Zhang, M. Xu, X. Zhou, H. Zhu, K. Zhang, *J. Mater. Chem. A* **2015**, *3*, 894.
[30] X. Li, J. Liu, M. N. Banis, A. Lushington, R. Li, M. Cai, X. Sun, *Energy Environ. Sci.* **2014**, *7*, 768.